Iraqi Journal of Physics, 2018 *Vol.16, No.36, PP. 140-152*
DOI: 10.20723/ijp.16.36.140-152

Dielectric properties of Li doped Ni-Zn ferrite

Mukhlis M. Ismail and Nasma A. Jaber

Department of Applied Sciences, University of Technology, Baghdad, Iraq

E-mail: nasmaadnanjaber@gmail.com

Abstract

Lithium doped Nickel-Zinc ferrite material with chemical formula $Ni_{0.9-2x}$ $Zn_{0.1}Li_xFe_{2+x}O_4$, where x is the ratio of lithium ions Li^+ (x = 0, 0.01, 0.02, 0.03 and 0.04) prepared by using sol-gel auto combustion technique. X-ray diffraction results showed that the material have pure cubic spinal structure with space group Fd-3m. The experimental values of the lattice constant (a_{exp}) were decreased from 8.39 to 8.35 nm with doped Li ions. It was found that the decreasing of the crystallite size with addition of lithium ions concentration. The radius of tetrahedral (r_{tet}) and octahedral (r_{oct}) site were computed from cation distribution. SEM images have been taken to show the morphology of compound. The dielectric parameters [dissipation factor (D_f), the dielectric constant (Ɛ') and a.c. conductivity (σ_{ac})] of spinal ferrite nano-powder have been measured. The dielectric parameters as a function of concentration have been studied for ferrite synthesis. The saturation of magnetization (M_s), remiensis (M_r) and coersivity (H_c) were found from hysteresis loop. The M_s and H_c varied from 36.47 to 66.15 emu/gm and 103 to 133 Oe for ferrite synthesis, respectively.

Key words
Lithium ferrite, dielectric constant, magnetic moment.

Article info.
Received: Sep. 2017
Accepted: Oct. 2017
Published: Mar. 2018

الخصائص الكهربائية للنيكل زنك فرايت المشوب بالليثيوم

مخلص مولود اسماعيل و نسمة عدنان جبر

قسم العلوم التطبيقية، الجامعة التكنولوجية، بغداد، العراق

الخلاصة

تم تحضير نيكل-زنك فرايت المشوب بأيونات الليثيوم باستخدام تقنية الاحتراق التلقائي (sol-gel auto combustion). من طيف الاشعة السينية تم حساب القيم العملية لثابت الشبيكة (a_{exp}) حيث وجد انه يقل مع إضافة ايونات الليثيوم بالإضافة الى النقصان في حجم البلورة. تم دراسة الخصائص الكهربائية كدالة للتردد ولقد وجد ان ثابت العزل والتوصيلية تقل مع زيادة التردد لكل العينات. لكن عند دراستها كدالة للتركيز فقد وجد ان هذه القيم تزداد مع اضافة الليثيوم. من حلقة الهسترة تم تحديد تمغنط الاشباع M_S وحساب القيم العملية والنظرية لعزوم التمغنط.

Introduction

Ferrite materials are insulating magnetic oxides and possess high electrical resistivity, low eddy current and dielectric losses, high saturation magnetization, high permeability and moderate permittivity [1]. The properties of ferrite can be modified by controlling the redistribution of metal ions at (A) and (B) sites; these are primarily responsible for the behavior of the magnetic ferrite. In addition, a kind of synthesis method can be designed to adjust the physical properties of ferrite by controlling the parameters such as PH value, concentration of component, and reaction of temperature and time. These methods can be assigned to solid-state reaction, hydrothermal, co-precipitation and sol-gel [2].

Prepare nanoparticle ferrites without any secondary phases or impurities must be taken into account maintaining the stoichiometry of the starting components that be achieved using sol-gel method [3]. Spinel ferrites are widely used in many electronic devices applications, such as memory devices, computer components and antenna rods. Ferrite materials are also used in biological (drug delivery, biosepration, magnetic resonance imaging and hyperthermia), catalysis, environmental and analytical applications [4].

Experimental

Lithium doped Nickel-Zinc ferrite nanoparticle with chemical formula $Ni_{0.9-2x}$ $Zn_{0.1}Li_xFe_{2+x}O_4$, where x is the ratio of lithium ions Li^+ (x = 0, 0.01, 0.02, 0.03 and 0.04) were prepared using sol-gel auto combustion technique. In this method, stoichiometric ratios of nickel nitrate $Ni(NO_3)_26H_2O$, zinc nitrate $Zn(NO_3)_26H_2O$, lithium nitrate $LiNO_3$, iron nitrate Fe $(NO_3)_3$ $9H_2O$ and citric acid $C_6H_8O_7$ the mole ratio of metal nitrates to iron nitrate to citric acid was taken as 1:2:3 which melted in appropriate amount of distilled water at room temperature and mixed by magnetic stirrer. After a short period, ammonia solution was added into the mixed solution to control its PH to reach the value to 7. The resulting sol was heated at 80 °C with constant stirring to form a wet gel. Dried the gel at 200 °C for one hour to form powder. For structural investigations as prepared samples were characterized by Rigaku (Ultima IV) X-ray diffractometer (XRD), scanning electron microscopy (SEM) model JEOL JSM-840. The dielectric measurements were carried out at room temperature using LCR Meter (Waynekerr Model: 43100) over the frequency range 100 Hz to 1 MHz. Since magnetic characterization was carried out using vibrating sample magnetometer VSM model EV-7, at room temperature.

Theory

By using, Braggs law the lattice parameters (a_{exp}) for cubic crystal calculated by the equation:

$$a_{exp} = d\sqrt{h^2 + k^2 + l^2} \quad (1)$$

where: d is the inter-planar distance, (*h k l*) are the miller indices, and (a_{exp}) is lattice constant, the crystallite size (D) was calculated from the full width at half-maximum (FWHM) using Williamson and Hall plot's [5], the equation is as following:

$$\beta \cos\theta = \delta\,(4\sin\theta) + \frac{\lambda}{D} \quad (2)$$

where β (FWHM in radian) is measured for different XRD lines corresponding to different planes, θ is the angle of Bragg diffraction, δ is the strain, λ is the wavelength of Cu-Kα (1.54 A°) and D is the crystallite size. Eq. (2) represents a straight line between 4sinθ (x-axis) and β cosθ (y-axis). The values of δ and D are obtained by the slope (δ) and intercept (λ/D). The theoretical values of lattice constant calculated by following equation [6]:

$$a_{th} = \frac{8}{3\sqrt{3}}\,(r_{tet} + R_O) + \sqrt{3}\,(r_{oct} + R_O) \quad (3)$$

The radius of oxygen ion is equal to (R_O= 1.38 A°), r_{tet} and r_{oct} are the radius of the tetrahedral and octahedral sites which determined from the ionic distribution according to the relations [7]:

$$r_{tet} = (0.1 - x)\,r_{Zn^{2+}} + (0.9 + x)\,r_{Fe^{3+}} \quad (4)$$

$$r_{oct} = \frac{1}{2}[(0.9 - 2x)r_{Ni^{2+}} + (x)r_{Li^{1+}} + (x)r_{Zn^{2+}} + (1.1)r_{Fe^{3+}}] \quad (5)$$

x is the lithium ions concentration and the values of the ionic radius are

($r_{Fe^{3+}} = 0.49$ A° for tetrahedral site, $r_{Fe^{3+}} = 0.645$A° for octahedral site, $r_{Ni^{2+}} = 0.69$ A°, $r_{Zn^{2+}} = 0.6$ A° for tetrahedral site, $r_{Zn^{2+}} = 0.74$ A° for octahedral site and $r_{Li^{2+}} = 0.73$ A°)[8-10].

The dielectric constant (ε') was calculated using the relation [11]:

$$\varepsilon' = Ct/\varepsilon_0 A \quad (6)$$

where C is the capacitance of the sample, t is the thickness; A is the surface area, and ε_o is the permittivity of free space ($\varepsilon_o = 8.85\times10^{-12}$ F/m). From dielectric constant and dissipation factor (D_f), the ac conductivity (σ_{ac}), of the ferrite samples can be calculated using the relation [12]:

$$\sigma_{ac} = 2\pi f \varepsilon'\varepsilon_0 D_f \quad (7)$$

where $\omega = 2\pi f$ is the angular frequency. The magnetic moment is calculated in Bhor magnetron using equation: [13]

$$(\mu_b)_{exp} = \frac{MM_S}{N_A \mu_B} \times 10^{-3} \quad (8)$$

where: M is molecular weight of particular composition in gm/mol.

M_S: is saturation magnetization in emu/gm.

N_A: is the Avogadro number $N_A = 6.022\times 10^{23}$ mol^{-1}.

μ_B: is Bohr magneton $\mu_B = 9.274 \times10^{-24}$ J/T and conversion factor 1emu = 10^{-3} J/T.

Results and discussion

The X-ray diffraction result of Lithium doped nickel-zinc ferrite nanoparticles samples are depicted in Fig. 1. The result analyzed by comparing it with standard {Joint Committee on Powder Diffraction Standards (JCDPS)} card. All peaks observed match well with JCPDS card no.52-0278 of the nickel-zinc ferrite for single-phase cubic spinel structure [14].

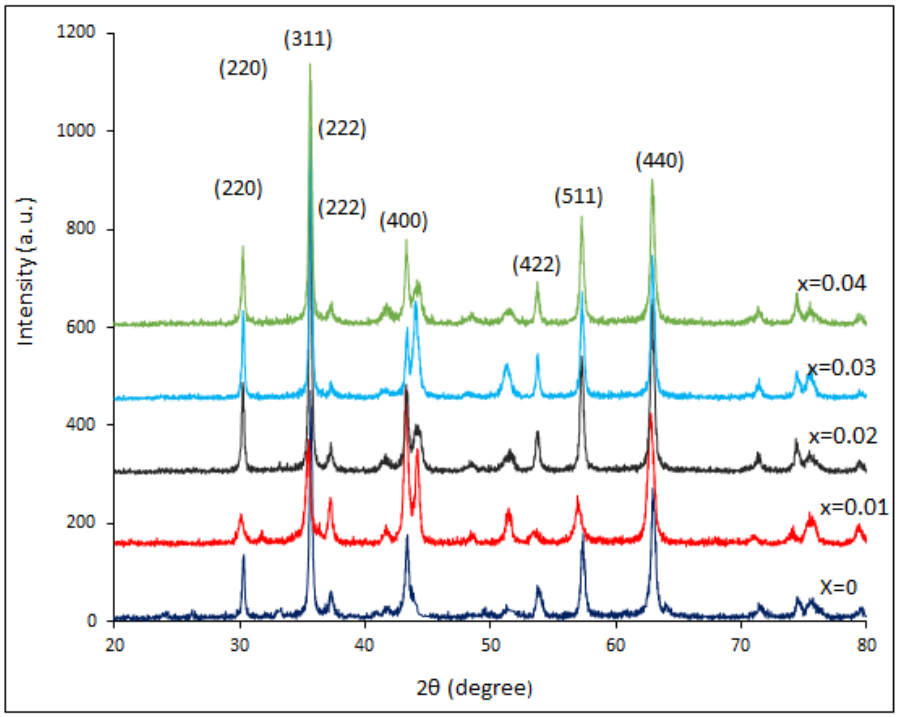

Fig. 1: XRD pattern of $Ni_{0.9-2x}Zn_{0.1}Li_xFe_{2+x}O_4$ {where x= 0, 0.01, 0.02, 0.03, 0.04}.

The peaks can be noted wide, this indicate the nature of nanoscale materials. The lattice parameter of as-prepared samples, according to the cubic crystal structure calculated from the main peak of spinel structure (311) using Eq. (1). Williamson and Hall (W-H) plots are used to calculate the crystallite size (D) from Eq. (2). Fig. 2 shows the linear fitting W-H plots. The values of strain (δ) was calculated from slop and (D) measured from intercept. The strain is neglected because it is small values.

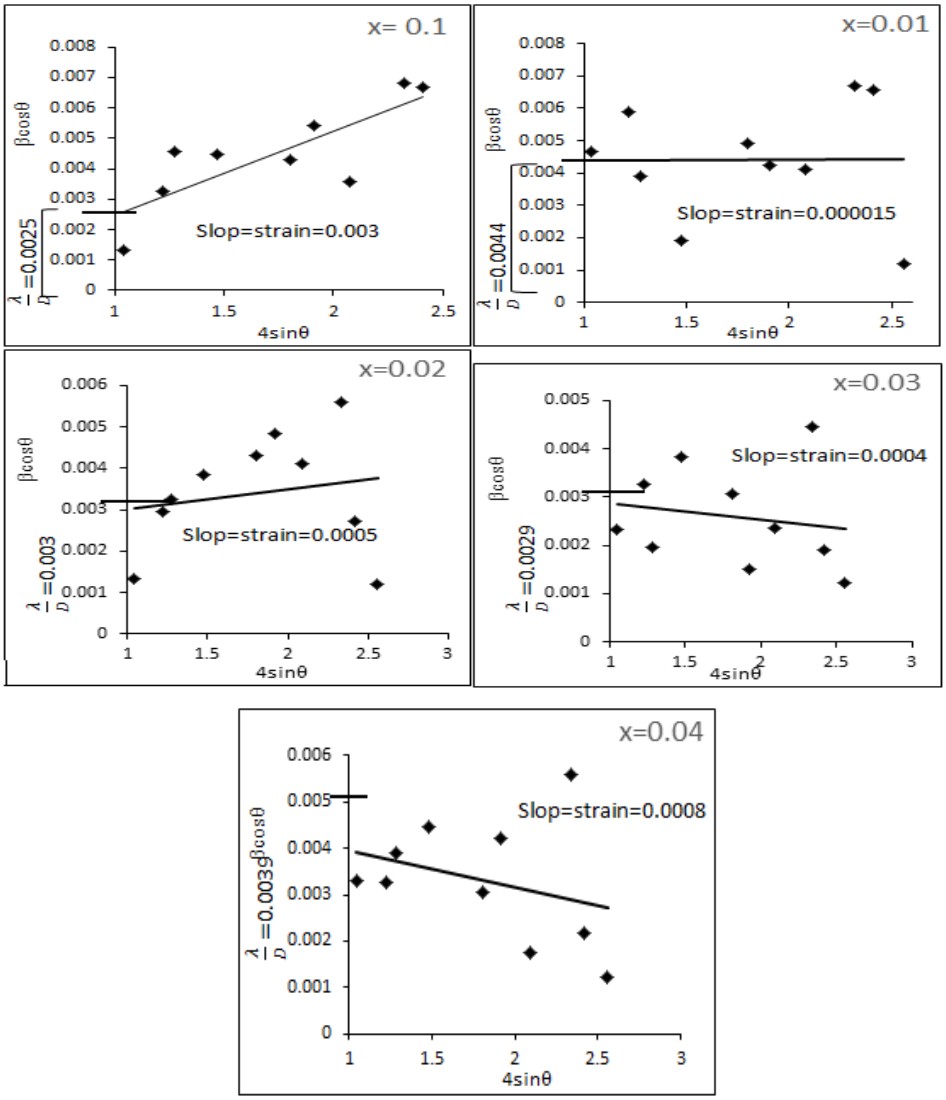

Fig. 2: Williamson and Hall plot graphs for $Ni_{0.9-2x}\ Zn_{0.1}Li_xFe_{2+x}O_4$ {where x= 0, 0.01, 0.02, 0.03, 0.04}.

The variation of lattice parameter and crystallite size with lithium ions concentration is shown in Fig. 3. The lattice constant values and the crystallite size decrease with doped lithium; this is attributed to large ionic radius value of lithium ion that occupy B-site (r_{Li}^{+} = 0.73 A°).

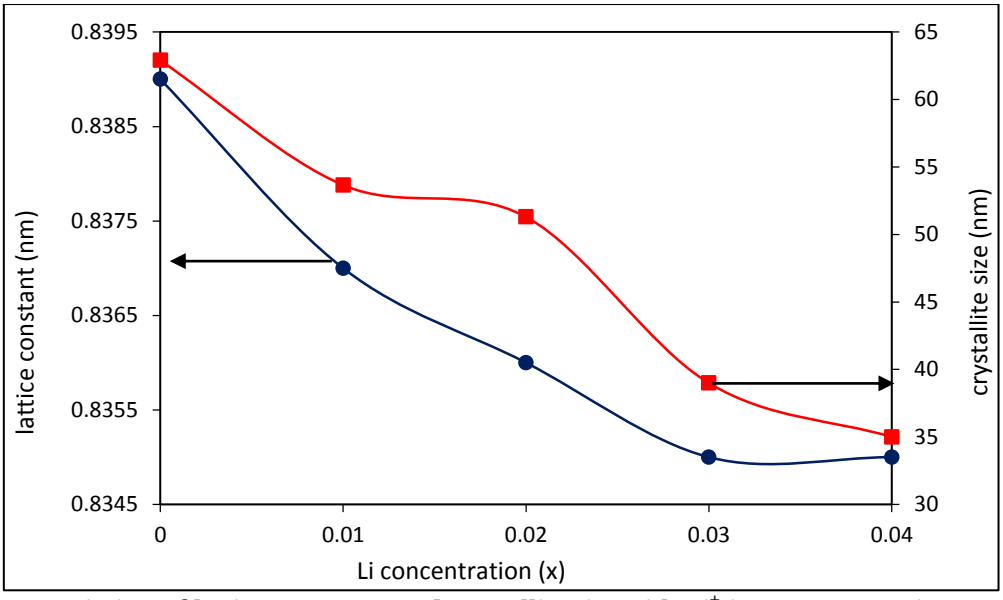

Fig. 3: Variation of lattice constants and crystallite size with Li^+ ions concentration.

The theoretically calculated values of the lattice constant according to the Eq. (3) are summarized in Table 1. These values are found in a good agreement with the experimental data. The radius of the tetrahedral and octahedral sites also calculated by relations (4) and (5). When doped with lithium the radius of A-site is decrease but the radius of b-site increase as show in Fig. 4.

Table 1: XRD pattern analysis of Li doped Ni-Zn ferrite. Experimental and theoretical lattice constant, crystallite size and the radius of the tetrahedral and octahedral sites.

x	a_{exp} (A°)	a_{th} (A°)	D (nm)	r_{tet} (A°)	r_{oct} (A°)
0	8.39	8.35	62.9	0.501	0.665
0.01	8.37	8.35	53.7	0.5	0.666
0.02	8.36	8.35	51.3	0.499	0.667
0.03	8.35	8.35	38.9	0.498	0.67
0.04	8.35	8.35	35	0.497	0.68

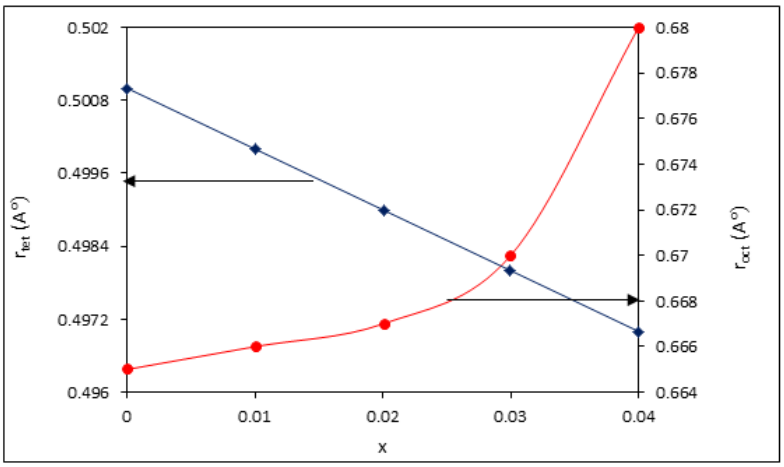

Fig. 4: Variation of tetrahedral and octahedral radius with lithium ions (x) concentration.

To show the morphology of sample the SEM images have been taken in Fig. 5. Note that the average grain size of the sample obtained from SEM images is larger than nanocrystals size, which determined by the XRD measurement, which simply indicates to the agglomeration in the nanoparticles. The samples are spherical, uniform and having a distribution size 62-101 nm.

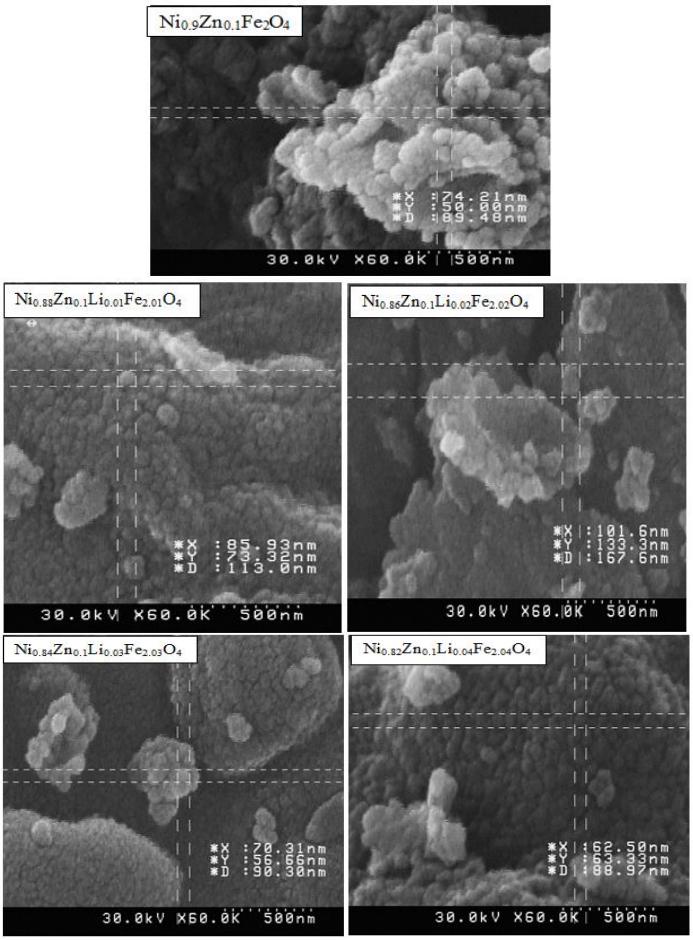

Fig. 5: SEM images of synthesized nickel-zinc-lithium ferrite nanoparticles.

The dissipation factor (D_f) of Li doped Ni-Zn ferrite as a function of frequency appear in Fig. 6.

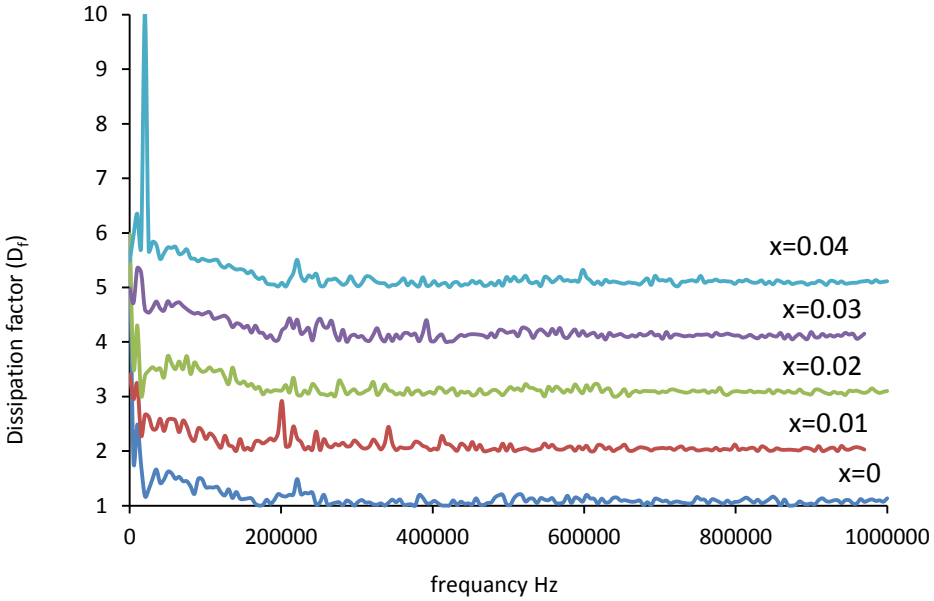

Fig. 6: Variation of dissipation factor with frequency for $Ni_{0.9-2x}Zn_{0.1}Li_xFe_{2+x}O_4$.

All the samples exhibit an abnormal behavior of peaking. There is a strong correlation between the conduction mechanism and dielectric behavior of the ferrites. The exchange of electrons between ferrous ions (Fe^{2+}) and ferric ions (Fe^{3+}) on the octahedral site may lead to local displacement of electrons in the direction of the applied field, and electrons determine the polarization. The dielectric loss in ferrites mainly originates due to the electron hopping and defect dipoles [15]. The electron hopping contributes to the dielectric loss only in the low-frequency range. The response of the electron hopping is decrease with increasing frequency, and hence, the dielectric loss decreases in the high-frequency range. The dielectric constant is a function of frequency can be seen in Fig. 7, which is decrease with increased frequency for all samples.

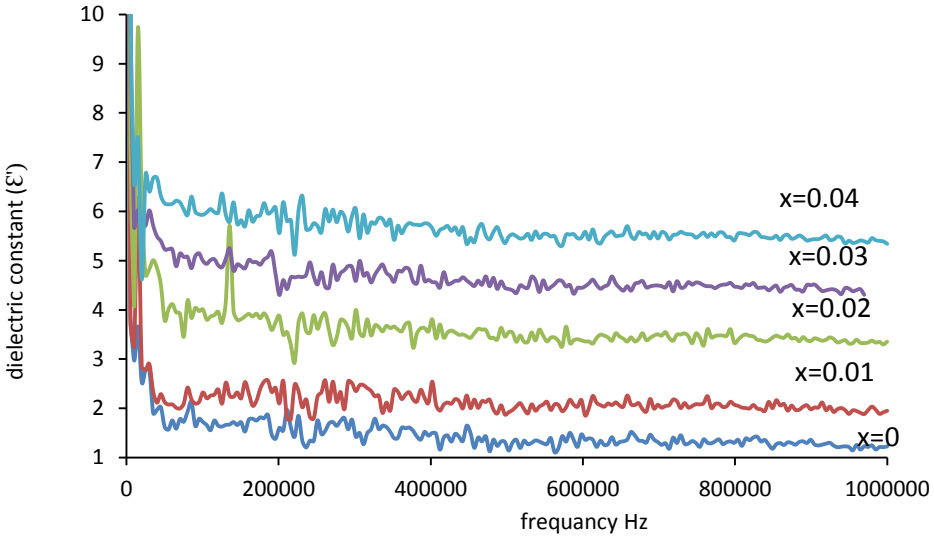

Fig. 7: Dielectric constant as a function of frequency for $Ni_{0.9-2x}Zn_{0.1}Li_xFe_{2+x}O_4$.

The ferrite composed of good conducting grains separated by poorly conducting grain boundaries. On the application of electric field, the electrons reach the grain boundary through hopping, and if the resistance of the grain boundary is high enough, electrons pile up at the grain boundaries and produce polarization. However, as the frequency of the applied external field is increased beyond a certain value, the hopping frequency cannot follow up the field variation.

It decreases the probability of the electrons reaching the grain boundary and as result polarization decreases which in turn causes to the decrement of dielectric constant. The large value of dielectric permittivity (ε') at low frequency is due to the domination of Fe^{2+} ions, oxygen vacancies, grain boundary defects, etc., while the decrease in ε' with frequency is due to the residue of species contributing to polarizability behind the applied electric field. At the higher frequencies ε' remains constant which is attributed to the contribution of electric polarizability only [16].

Variation of a.c. conductivity with frequency exhibit in Fig. 8, all the curves; exhibit the significant dispersion with frequency, which is an important behavior of ferrites.

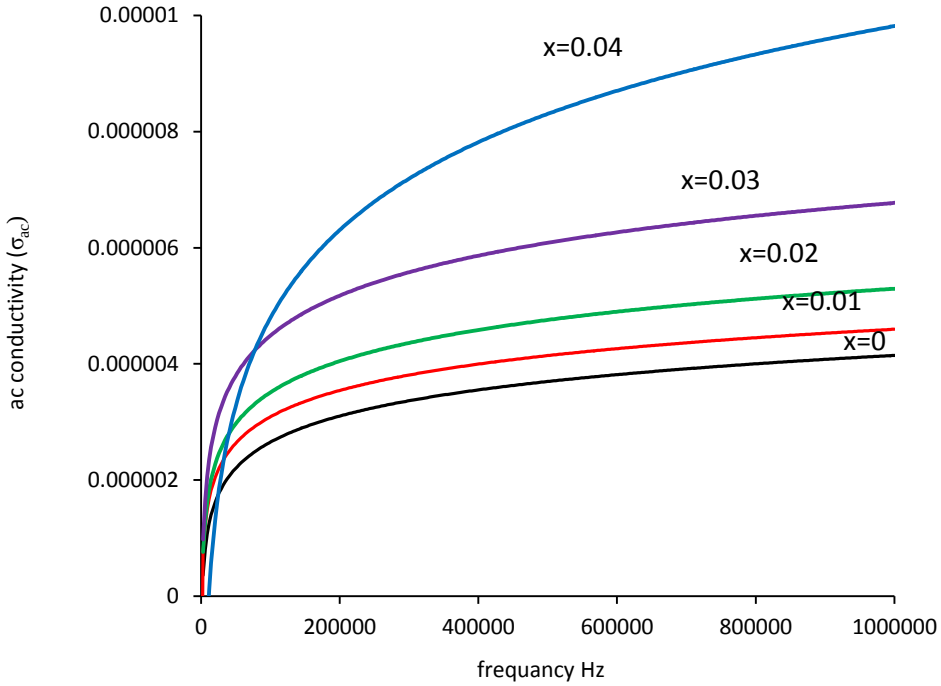

Fig. 8: a.c. conductivity as a function of frequency for $Ni_{0.9-2x}Zn_{0.1}Li_xFe_{2+x}O_4$.

The electrical conductivity in ferrites is mainly due to the hopping of electrons between the ions of the same element presented in more than one valence state and distributed randomly over crystallography equivalent lattice sites [17]. The dielectric parameters for lithium doped Ni-Zn ferrite increase with Li ions concentration. The value of these parameters have been taken at frequency 5×10^5 Hz as show in Table 2, the variation of dielectric constant and ac conductivity can be note in Fig. 9. These variations refer to the change in the number of ferrous ions on the octahedral sites, which plays a dominant role in the mechanisms of conduction and dielectric polarization.

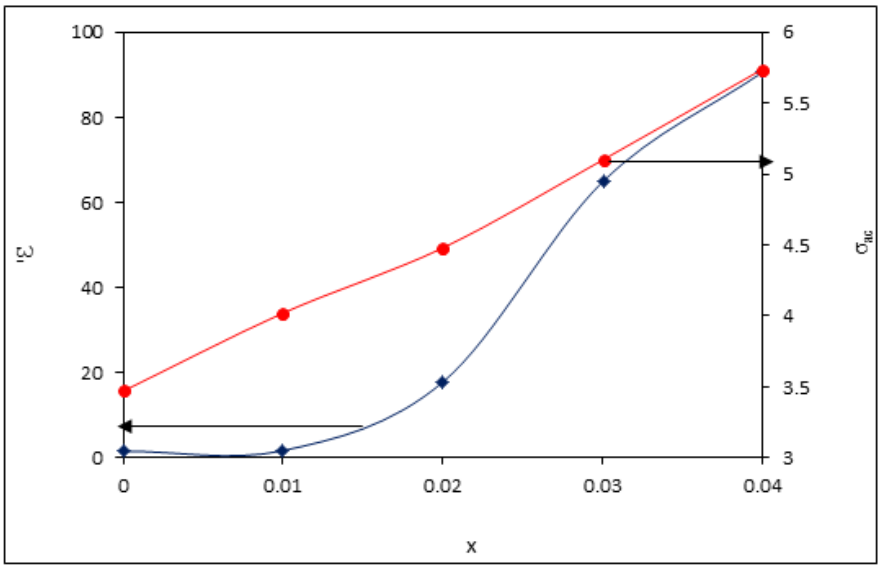

Fig. 9: The dielectric constant and a. c. conductivity as a function of concentration for $Ni_{0.9-2x}Zn_{0.1}Li_xFe_{2+x}O_4$ ***{where x= 0, 0.01, 0.02, 0.03, 0.04}.***

Table 2: Dielectric properties (capacitance (C), dissipation factor (D), dielectric constant (Ɛ') and ac conductivity (σ_{ac}) ***as a function of composition at frequency*** 5×10^5 ***Hz.***

x	C(F)×10^{-12}	D_f	Ɛ'	σ_{ac} ×10^{-6} s/cm
0	1.22	0.1665977	1.58	3.47
0.01	1.06	0.172	1.69	4.02
0.02	13.6	0.175	17.8	4.48
0.03	47.7	0.207	64.9	5.10
0.04	69.7	0.21	90.6	5.74

The hysteresis loop of Li doped Ni-Zn ferrite show in Fig. 10, the loop is narrow which means the papered samples are soft magnetic material.

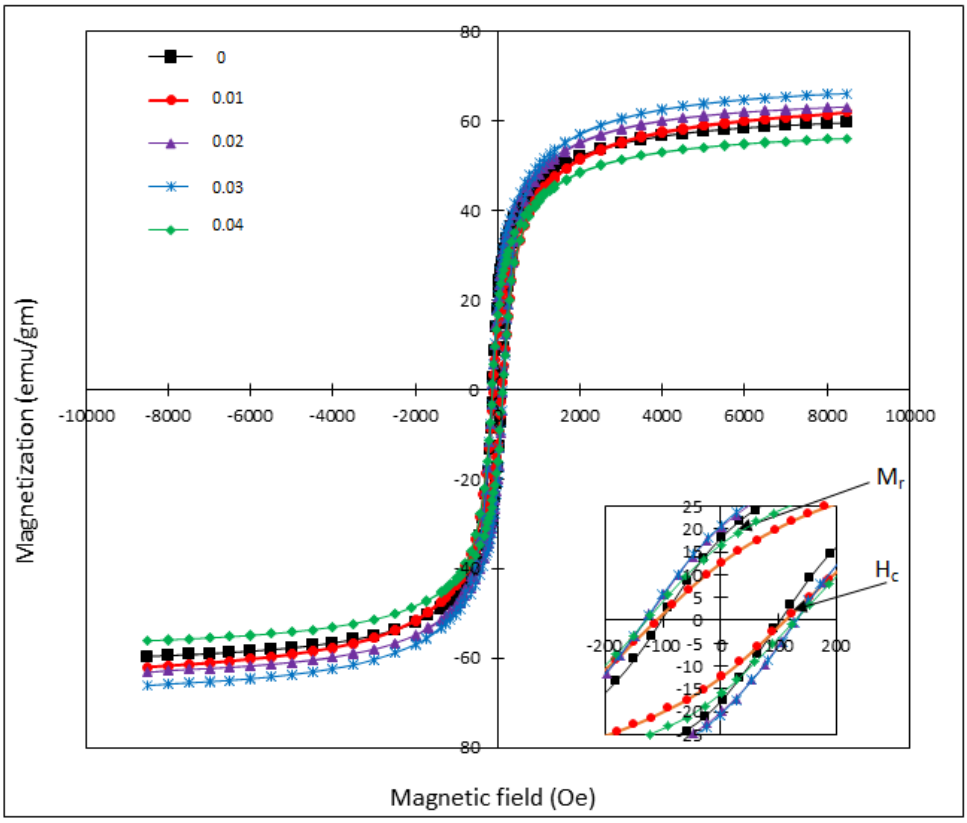

Fig.10: Magnetic hysteresis loops of $Ni_{0.9-2x}Zn_{0.1}Li_xFe_{2+x}O_4$ (x=0, 0.01, 0.02, 0.03 and 0.04).

The saturation magnetization (M_s) and coercivity (H_C) values have been directly extracted from these curves as in insert of Figure and listed in various Li content in Table 3. The saturation magnetization and coercivity increase with Lithium content and then decrease after y=0.03, the behavior of the saturation magnetization can be explained because of cations distribution and super-exchange interactions.

The relationship between the magnetic properties and Li ions concentration can be seen clearly in Fig.11, where M_s and H_C values are plotted against Li^+ concentration (x).

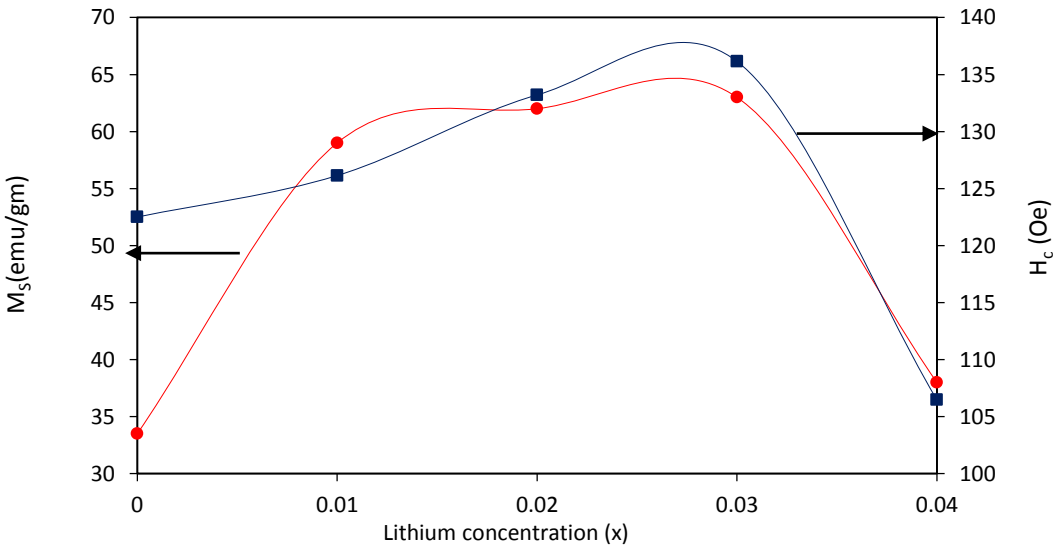

Fig. 11: Change of saturation magnetization and coercivity with Li ions concentration.

From Table 3, the magnitude of magnetic moment is decrease and then increase with Li content because of the increase the A-B interaction between two sites. The magnetic moments determined by the number of ions in A and B sites of the spinal ferrite. The magnetic properties of samples have been determined by a net magnetization to the sub lattice site according to Neel model. The size of octahedral site is larger than tetrahedral site, therefore the largest ionic radius, moving towards B-site, the cations distribution formula of Ni-Zn ferrite is:

$$(Zn_{0.1}^{2+}Fe_{0.9}^{3+})_{tet}[Ni_{0.9}^{2+}Fe_{1.1}^{3+}]_{oct}O_4$$

Theoretically, the magnitude of magnetic moment can be calculated by the equation $\mu_{th} = \mu_{oct} - \mu_{tet}$ so from cation formula and moment of each ion (Zn^{2+}=0, $Fe^{3+} = 5\mu_B$ and $Ni^{2+} = 2\mu_B$) therefore μ_{th} is equal to 2.8 μ_B which is larger than the experimental values (2.2 μ_B). After doping Ni-Zn-ferrite with Li^+ ions, the Ni^{2+} ions are replaced in the octahedral site, which led to increase Fe^{3+} ions in tetrahedral sites by the same quantity to obtain electrical neutrality. Increase in the amount of iron ions in tetrahedral site leads to push the zinc ions from A-site to B-site and the cation distribution of Ni-Li-Zn spinal can be rewritten as the following:

$$(Zn_{0.1-x}^{2+}Fe_{0.9+x}^{3+})_{tet}\,[Ni_{0.9-2x}^{2+}Li_x^{+}Zn_x^{2+}Fe_{1.1}^{3+}]_{oct}O_4$$

In addition, the Theoretical values of magneting moment μ_{th} decrease. Comparison between experimental and theoretical values of magnetic moment can be seen in Fig. 12. The redistribution of the cations between two sites led to an increase of the net magnetic moment, saturation magnetization, remanence and coercivity with doping of lithium.

Table 3: The values of saturation magnetization, remanence, coercivity and magnetic moment of fer.

x	M_s (emu/gm)	M_r (emu/gm)	H_c (Oe)	$(\mu_B)_{theor}$	$(\mu_B)_{exp}$
0	52.5	16.4	103.5	2.8	2.2
0.01	56.14	16.8	129	2.72	2.34
0.02	63.21	20.4	132	2.64	2.6
0.03	66.15	20.8	133	2.62	2.7
0.04	36.47	7.4	108	2.56	1.53

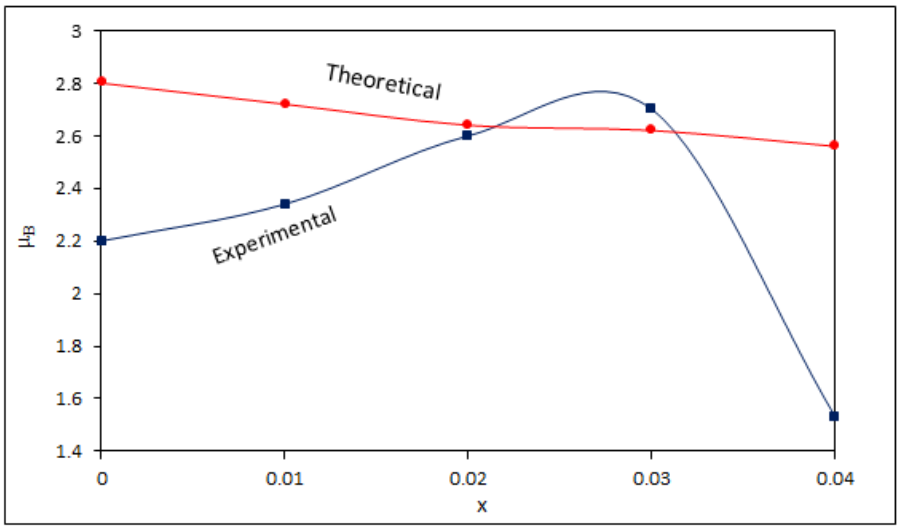

Fig. 12: The variation of magnetic moment with Li concentration.

Conclusions

The lattice constant decrease with doped lithium and the crystallite size of the sample change with Li doping (x). The change in values of the radius of the tetrahedral and octahedral sites when doped with lithium ions means effect on distance between ions and cation distribution between two sites. The dielectric properties decrease as a function of frequency this make the samples suitable for high frequency applications. The saturation magnetization, coercivity and remanence of the material varied by addition of Li ions. There is a big difference between the practical and theoretical values of the moments for Ni-Zn- Li ferrite and the cation distribution effect on magnetic properties.

References

[1] B. D. Cullity and C. D. Graham, "introduction to magnetic materials", 2nd Ed, John Wiley and Sons, ch.6, 175-196, 2009.

[2] A. Goldman, "Modern ferrite technology", 2nd Ed., Springer, ch.4, 51-66, 2006.

[3] K.H.J. Buschow, "Handbook of Magnetic Materials", Elsevier, ch.3, 107-189, 2008.

[4] P. Venugopal Reddy and T. Seshagiri Rao, J. of the Less-Common Metals, 86, 3 (1982) 255-261.

[5] R. Peelamedu, C. Grimes, D. Agrawal, R. Roy, J. Mater. Res., 18, 6 (2003) 2292 -2295.

[6] P.K. Roy and J. Bera, Elsevier, 197, 26 (2008) 279-283.

[7] N. H. Kumar, N. Venkatesh, G. Aravind, S. Goud, T. Somaiah, D. Ravinder, J. Appl. Phys., 7, 1 (2015) 79-83.

[8] N. Rezlescu and E. Rezlescu, J. Appl. Phys., 7, 19 (1997) 219-225.

[9] K. R. Krishna and D. Ravinder, J. Phys. Chem., 2, 23 (2012) 185-191.

[10] I. Soibam, N. Nilima, S. Phanjoubam, American Journal of Materials Science and Engineering, 2, 1 (2014) 24-27.

[11] Y. Hayashimto, W. Sakamoto, T. Yogoa, J. Mater. Res., 22, 16 (2007) 1967-1974.

[12] T. Zhou, D. Zhang, Lijun Jia, Feiming Bai, Lichuan Jin, J. Phys. Chem., 119, 77 (2015) 13207-13214.

[13] A. Kumar, P. Kumar, M. Kumar, J. Appl. Phys., 09, 11 (2014) 228-230.

[14] S. A. Mazen and T. A. Elmosalami, Conde. Matt. Phys., 9, 4 (2011) 820726-820733.

[15] G. S. V. R. K. Choudary, M. C. Varma, K. H. Rao, Indian Journal of

Research in Pharmacy and Biotechnology, 1, 7 (2014) 36-41.
[16] Y. Liu, S. C. Wei, Y. J. Wang, H. L. Tian, H. Tong, B. S. Xu, Physics Procedia, 50, 12 (2013) 43-47.
[17] Z. Peng, Xiuli Fu, Huilin Ge, Zhiqiang Fu, C. Wang, Longhao Qi, H. Miao, J. of magnetism and Magnetic Materials, 323, 123 (2011) 2513-2518.